



UNIVERSIDADE ESTADUAL DE CAMPINAS  
SISTEMA DE BIBLIOTECAS DA UNICAMP  
REPOSITÓRIO DA PRODUÇÃO CIENTÍFICA E INTELLECTUAL DA UNICAMP

**Versão do arquivo anexado / Version of attached file:**

Versão do Editor / Published Version

**Mais informações no site da editora / Further information on publisher's website:**

<https://academic.oup.com/jge/article/17/6/929/5956271>

**DOI: 10.1093/jge/gxaa053**

**Direitos autorais / Publisher's copyright statement:**

©2020 by Oxford University Press. All rights reserved.

DIRETORIA DE TRATAMENTO DA INFORMAÇÃO

Cidade Universitária Zeferino Vaz Barão Geraldo

CEP 13083-970 – Campinas SP

Fone: (19) 3521-6493

<http://www.repositorio.unicamp.br>

# Comparing different approaches of time-lapse seismic inversion

**Daiane R. Rosa<sup>1,\*</sup>, Juliana M. C. Santos<sup>1</sup>, Rafael M. Souza<sup>2</sup>, Dario Grana<sup>3</sup>, Denis J. Schiozer<sup>1</sup>, Alessandra Davolio<sup>1</sup> and Yanghua Wang<sup>4</sup>**

<sup>1</sup> Faculty of Mechanical Engineering, University of Campinas, Mendeleev Street, 200, Campinas, SP, 13083–860, Brazil

<sup>2</sup> Centre for Energy Geoscience, School of Earth Sciences, The University of Western Australia, 35 Stirling Highway, Perth, WA, 6009, Australia

<sup>3</sup> Department of Geology & Geophysics, University of Wyoming, 1000 E. University Avenue, Laramie, WY 82071, USA

<sup>4</sup> Resource Geophysics Academy, Department of Earth Science and Engineering, Imperial College London, London SW7 2BP, UK

\*Corresponding author: Daiane R Rosa. E-mail: [daiane@cepetro.unicamp.br](mailto:daiane@cepetro.unicamp.br)

Received 4 March 2020, revised 5 August 2020

## Abstract

Time-lapse (4D) seismic inversion aims to predict changes in elastic rock properties, such as acoustic impedance, from measured seismic amplitude variations due to hydrocarbon production. Possible approaches for 4D seismic inversion include two classes of method: sequential independent 3D inversions and joint inversion of 4D seismic differences. We compare the standard deterministic methods, such as coloured and model-based inversions, and the probabilistic inversion techniques based on a Bayesian approach. The goal is to compare the sequential independent 3D seismic inversions and the joint 4D inversion using the same type of algorithm (Bayesian method) and to benchmark the results to commonly applied algorithms in time-lapse studies. The model property of interest is the ratio of the acoustic impedances, estimated for the monitor, and base surveys at each location in the model. We apply the methods to a synthetic dataset generated based on the Namorado field (offshore southeast Brazil). Using this controlled dataset, we can evaluate properly the results as the true solution is known. The results show that the Bayesian 4D joint inversion, based on the amplitude difference between seismic surveys, provides more accurate results than sequential independent 3D inversion approaches, and these results are consistent with deterministic methods. The Bayesian 4D joint inversion is relatively easy to apply and provides a confidence interval of the predictions.

**Keywords:** 4D seismic inversion, Bayesian inversion, deterministic inversion, probabilistic inversion, time-lapse seismic

## 1. Introduction

Time-lapse (4D) seismic data are a valuable source of information for monitoring and managing the production of hydrocarbon reservoirs. The processing and interpretation of 4D data include the calculation and evaluation of the changes in seismic attributes (e.g., seismic amplitude,

acoustic impedance, P and S-wave velocities and density) resulting from changes in reservoir pressure, fluid saturation and temperature caused by reservoir production (Johnston 2013). Thus, 4D seismic attributes provide a useful spatial constraint to the updating of reservoir properties within simulation model grids and enable the mitigation of potential reservoir management risks.

In the context of dynamic reservoir modelling, 4D seismic data are used to update the simulation model, manually or automatically, in history matching studies (Ullmann de Brito *et al.* 2010; Oliver & Chen 2010; Davolio *et al.* 2014). In common industry practices, once 4D seismic data are inverted to estimate elastic properties, then the results obtained are assimilated in the dynamic fluid flow simulation workflow.

The goal of seismic inversion is to determine a reservoir model that minimises the errors between the predicted seismic amplitudes and the observed seismic amplitudes (Wang 2003; Francis 2005). Seismic inversion methods for reservoir characterisation can be divided into two main categories: deterministic and probabilistic approaches. Deterministic methods generally provide a single solution, constrained by a prior model or well data, and include, among others, coloured and model-based inversions (Simm *et al.* 2014). Maurya & Sarkar (2016) compared the results of model-based, coloured, sparse-spike and band-limited inversions in 3D seismic data from the Blackfoot field (Alberta, Canada), and concluded that all methods produce accurate and reliable results. Probabilistic methods are based on mathematical formulations that are generally more adequate at representing the non-uniqueness of the solution to the inverse problem. The solution is expressed by probability distributions or by a set of multiple realisations that are consistent with the observed seismic data (Bacon *et al.* 2007). The results represent not only the most likely model, but also the model uncertainty. A commonly adopted probabilistic method in reservoir characterisation is the Bayesian inversion, which allows evaluating the impedance of the most likely model and its uncertainty (Buland & Omre 2003) by combining a priori information on model parameters with the measured data in a probabilistic formulation. The Bayesian inversion (Buland & Omre 2003) was then extended to time-lapse studies (Buland & El Ouair 2006) and other geophysical applications (Grana & Mukerji 2015; Veire *et al.* 2006) to estimate reservoir rock properties. The limitations of the deterministic methods are highlighted in Francis (2005), in the comparison with realisations of a probabilistic method, showing a significant underprediction of net sands in the deterministic inversion due to the smoother estimated impedances, whereas the probabilistic inversion better reproduces the impedance distribution.

For 4D seismic inversion, a common practice is to independently invert the base and repeated 3D seismic surveys using seismic inversion methods, and then obtain the changes in impedances from the difference of the results. Alternatively, one can compute the difference of seismic amplitudes between the base and repeated 3D seismic surveys and then apply a joint seismic inversion method directly to the difference of seismic data. There is also the simultaneous approach, where all surveys are combined in a single objective function, with an optimised 4D solution that matches

the available data. Lafet *et al.* (2008) proposed a 4D inversion approach where data of multiple vintages were inverted simultaneously in the Brage Field (Norway), showing that the impedance results were more accurate with respect to the expected water flood effects when compared to sequential independent 3D inversions of base and monitor surveys. Sarkar *et al.* (2003) showed that joint seismic inversion has a lower computational cost compared to sequential independent 3D inversions, and requires a single wavelet and a simpler initial model, which represents the changes in acoustic impedances between different surveys. Another advantage is that it allows access to 4D results directly in the interactive process of parametrisation.

The objective of this study is to compare different seismic inversion techniques to predict changes in the acoustic impedance. The methods we used are: (i) sequential independent 3D inversions using the Bayesian method (Buland & Omre 2003); (ii) joint inversion of 4D differences using the Bayesian method (Buland & El Ouair 2006) and (iii) sequential independent 3D inversions using deterministic methods. For the deterministic methods we adopted two common approaches, namely coloured and model-based inversions (Kazemi *et al.* 2011; Maleki *et al.* 2018; Najjar *et al.* 2003). The proposed analysis aims to investigate the difference between the independent and joint approaches of the Bayesian inversion through a fair comparison with well-known deterministic methods. The results are expressed as a percentage of the impedance changes between base and repeated surveys to compare the same model variable in all the cases. The application is performed in a synthetic case, where the true solution (acoustic impedance) is known at all time steps, and an accurate comparison can be made between the inverted impedances and the reference values. The dataset of UNISIM-I-D (Avansi & Schiozer 2015) is based on real data of the Namorado field (Campos Basin, Brazil). Two synthetic seismic surveys, baseline (pre-production) and monitor (after seven years of production) were generated as described in Souza *et al.* (2018).

## 2. Basics of 4D seismic inversion

Seismic inversion aims to predict the subsurface elastic parameters  $\mathbf{m}$  from the acquired seismic data  $\mathbf{S}$ . If the seismic forward model is linear, the mathematical formulation of the forward problem (Grana & Mukerji 2015) can be written as

$$\mathbf{S} = \mathbf{G}\mathbf{m} + \mathbf{e}_s, \quad (1)$$

where  $\mathbf{S}$  is the vector of seismic amplitudes,  $\mathbf{G}$  is the matrix associated to the forward linearised model,  $\mathbf{m}$  is the vector of elastic parameters (e.g., acoustic impedance) and  $\mathbf{e}_s$  is a random error with a normal distribution with zero mean and known covariance matrix. In the convolutional linearised approximation, the forward linear model  $\mathbf{G}$  can also be written

as  $\mathbf{G} = \mathbf{WAM}$ , where  $\mathbf{W}$  is the matrix of wavelets,  $\mathbf{A}$  the reflection coefficients computed with a linear approximation of the Zoeppritz equations (Aki & Richards 1980; Wang 1999) and  $\mathbf{M}$  is a first-order differential matrix (Buland & Omre 2003). The corresponding inverse problem for the prediction of  $\mathbf{m}$  given  $\mathbf{S}$  can be solved using different mathematical inversion and optimisation methods (Tarantola 2005). In our study, we only consider the acoustic case. It is important to notice that the linearisation is obtained in terms of the logarithm of impedance ( $\mathbf{m} = \ln \mathbf{IP}$ ) (Buland & Omre 2003). This formulation can be applied any time when seismic data are available and only requires a prior model of the acoustic impedance and the source wavelet.

In 4D inversion studies, the goal is to predict the changes in acoustic properties between two seismic surveys, the based and the repeated surveys. One can perform multiple inversions (i.e. sequential independent 3D inversion method), by independently solving the following seismic inversion problems

$$\mathbf{S}_{\text{base}} = \mathbf{G}_{\text{base}} \mathbf{m}_{\text{base}} + \mathbf{e}_{\text{base}}, \quad (2)$$

$$\mathbf{S}_{\text{monitor}} = \mathbf{G}_{\text{monitor}} \mathbf{m}_{\text{monitor}} + \mathbf{e}_{\text{monitor}}, \quad (3)$$

where the final solution is  $\Delta \mathbf{m} = \mathbf{m}_{\text{monitor}} - \mathbf{m}_{\text{base}}$ .

Alternatively, we can formulate the problem as a joint inversion applied to the difference of seismic data (i.e. joint 4D inversion of the difference), assuming the same modelling operator  $\mathbf{G}$ :

$$\Delta \mathbf{S} = \mathbf{S}_{\text{monitor}} - \mathbf{S}_{\text{base}} = \mathbf{G} \Delta \mathbf{m} + \mathbf{e}_{\text{it}}. \quad (4)$$

In the case of the joint Bayesian 4D seismic inversion (Buland & El Ouair 2006), for seismic data with incident angle equal to 0, the vector  $\Delta \mathbf{m}$  of elastic parameter changes is written as

$$\Delta \mathbf{m} = \ln \frac{\mathbf{IP}_{\text{monitor}}}{\mathbf{IP}_{\text{base}}}, \quad (5)$$

and the acoustic impedance changes are evaluated as

$$\exp(\Delta \mathbf{m}) = \frac{\mathbf{IP}_{\text{monitor}}}{\mathbf{IP}_{\text{base}}}, \quad (6)$$

where  $\mathbf{IP}$  is the acoustic impedance.

In our comparison, we use the 3D Bayesian inversion proposed in Buland & Omre (2003) to sequentially solve the inverse problems in equations (2) and (3) and the joint 4D Bayesian inversion of the seismic differences in Buland & El Ouair (2006) to solve the inverse problem in equation (4). Both methods are probabilistic, and provide the posterior distribution of the model parameters. In both approaches, the forward modelling is based on the convolution of the wavelet and a linearised weak contrast reflectivity function defined for continuous seismic travel time. The solution is represented by a Gaussian posterior distribution with posterior mean and covariance matrix. The result of the Bayesian

4D joint inversion is the natural logarithm of the ratio between acoustic impedance from the monitor and acoustic impedance from the base (equation (5)).

Seismic inversion requires a low-frequency model of impedance due to the limited bandwidth of seismic data. In Bayesian 3D inversion, the low-frequency model (in the logarithmic domain) is the mean of the prior distribution (Buland & Omre 2003). In Bayesian 4D joint inversion, the prior model is instead expressed as the logarithm of the ratio  $\mathbf{IP}_{\text{monitor}}/\mathbf{IP}_{\text{base}}$ . If no information about the dynamic changes is available, the initial model is set to zero everywhere (Buland & El Ouair, 2006).

The two discussed Bayesian methods are then compared to standard deterministic methods. The model-based inversion (Russell & Hampson 1991; Wang 2016) consists of minimising the difference between the modelled and the observed seismic traces using the least-squares optimisation technique. Because the reflection coefficients describe the relative contrast between the elastic properties in the layers above and below the interface, the inversion only provides information about the changes in the elastic properties, i.e. P-impedance. Therefore, a low-frequency model of P-impedance must be assumed. Generally, this model is constructed by interpolating well log data between seismic horizons. The seismic wavelet is estimated from well data. The impedance model is solved iteratively by perturbing the initial model until the lowest misfit between observed and predicted data is achieved.

Alternatively, coloured inversion (Lancaster & Whitcombe 2000) is a method performed in the frequency domain and designed to approximately match the spectrum of seismic data with the spectrum of impedance. This inversion does not require an initial low-frequency model but it requires zero-phased seismic data (Veeken & Da Silva 2004). An operator spectrum is calculated from the combination of the acoustic impedance spectrum from wells and the seismic spectrum of traces close to the wells. After taking the average impedance spectrum, a  $-90^\circ$  phase shift is applied so that the operator is created in the time domain, and convoluted with the seismic trace to generate acoustic impedances (Maurya & Sarkar 2016).

### 3. Comparison of various inversions

The goal of this work is to compare the sequential independent 3D inversion method and the joint 4D inversion of the difference in the Bayesian and deterministic context, with deterministic seismic inversions commonly used in 4D studies.

Figure 1 illustrates the steps to compare different inversion results with respect to the true solution. The orange box highlights the steps needed to generate the synthetic seismic data (synthetic seismic amplitudes). The blue boxes show the

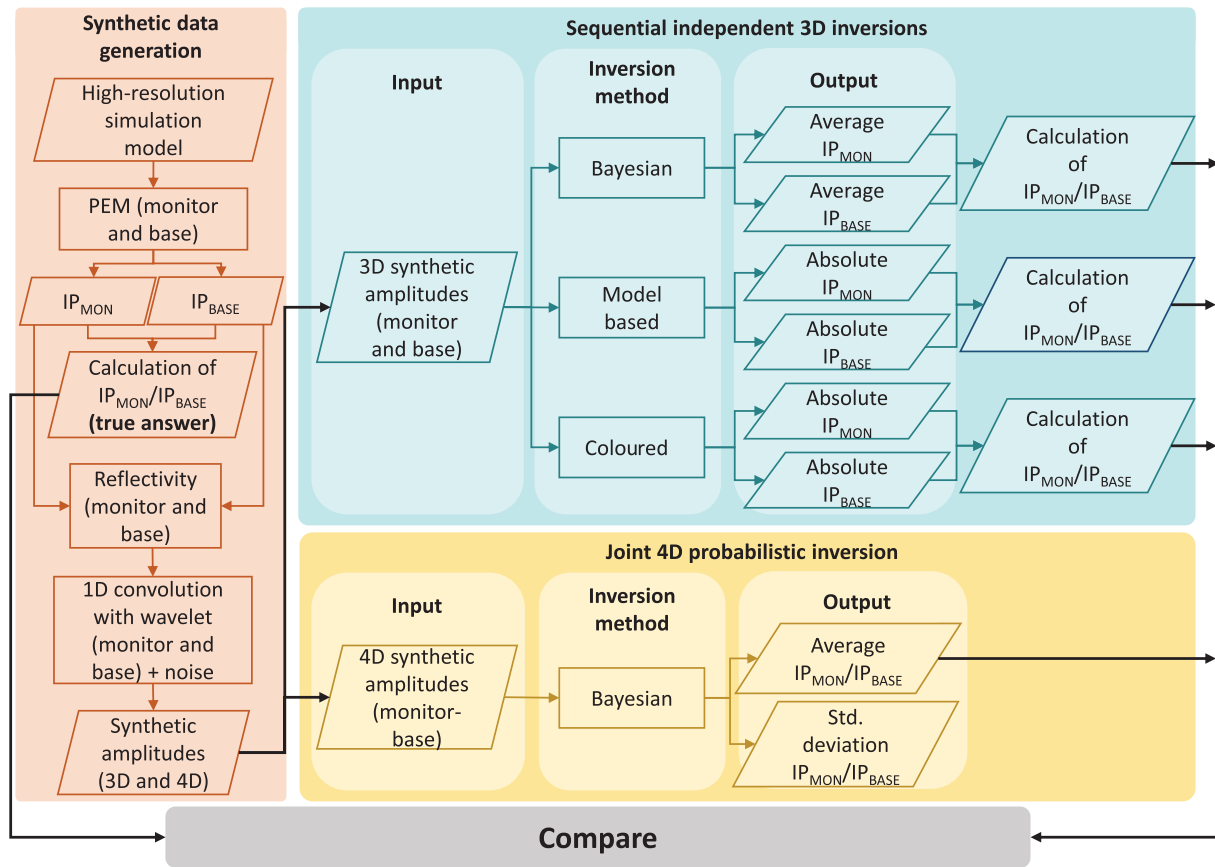


**Figure 1.** Tasks performed for seismic forward modelling and for each inversion method: deterministic (model-based and coloured) and probabilistic (Bayesian) 3D and 4D; and comparison with the true model.

sequential independent 3D inversions and the yellow boxes show the joint 4D inversion. The procedures for model-based and coloured inversions were performed using the commercial Hampson-Russell software (CGG 2016). The Bayesian inversion was implemented in a prototype MATLAB code (Grana & Mukerji 2015). The absolute values of optimised models obtained by deterministic methods and the mean values of Bayesian 3D inversions are used to calculate acoustic impedance ratios between baseline and repeated surveys for each method, and compared to the mean acoustic impedance ratio ( $IP_{\text{monitor}}/IP_{\text{base}}$ ) that is derived from the probabilistic Bayesian 4D joint method.

The comparison between seismic inversions is carried qualitatively by visually analysing maps and vertical sections and quantitatively with statistical indicators that measure the proximity of each inversion method to the true solution. Common indicators include linear correlation, densities and cumulated probability curves. An alternative statistical analysis for the quantitative interpretation is to calculate the similarity between maps of inversion results and true data. Rollmann *et al.* (2020) proposes using the pixel-wise metric, mean square error (MSE), for standardised maps to

properly calculate the error to the reference data. The MSE standard property is defined as:

$$Z = \frac{A - \mu}{\sigma}, \tag{7}$$

where  $\mu$  is the mean of values of the predicted property  $A$  and  $\sigma$  is the standard deviation. The traditional pixel-wise metric MSE measures the misfit between normalised property  $Z$  and reference property  $B$ :

$$MSE = \frac{1}{N} \sum_{i=0}^N (Z_i - B_i)^2, \tag{8}$$

where  $N$  is the number of points in the data.

#### 4. Application

The benchmark dataset UNISIM-I is based on the Namorado field, a sandstone reservoir located in the Campos basin, Brazil (Avansi & Schiozer 2015). In this synthetic dataset, a high-resolution numerical model represents the true subsurface model. Water injection is the production strategy to keep reservoir pressure above the bubble point

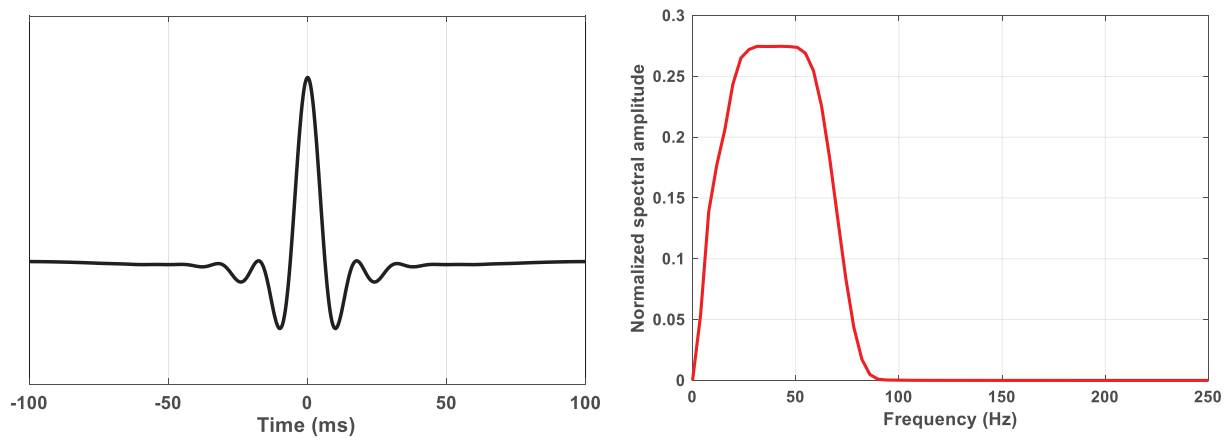


Figure 2. The Ormsby wavelet used to generate synthetic seismic data and inversion results (left) and its frequency spectrum (right).

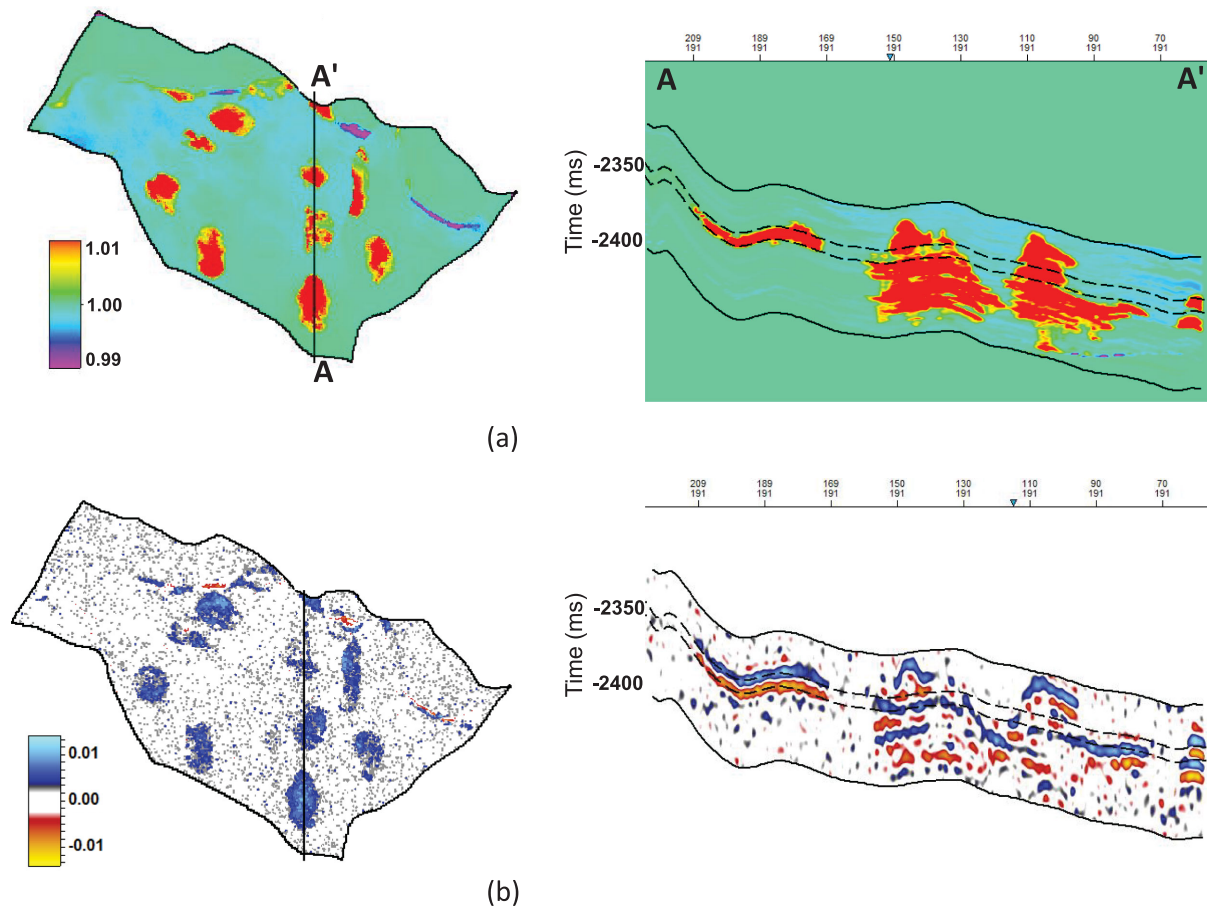
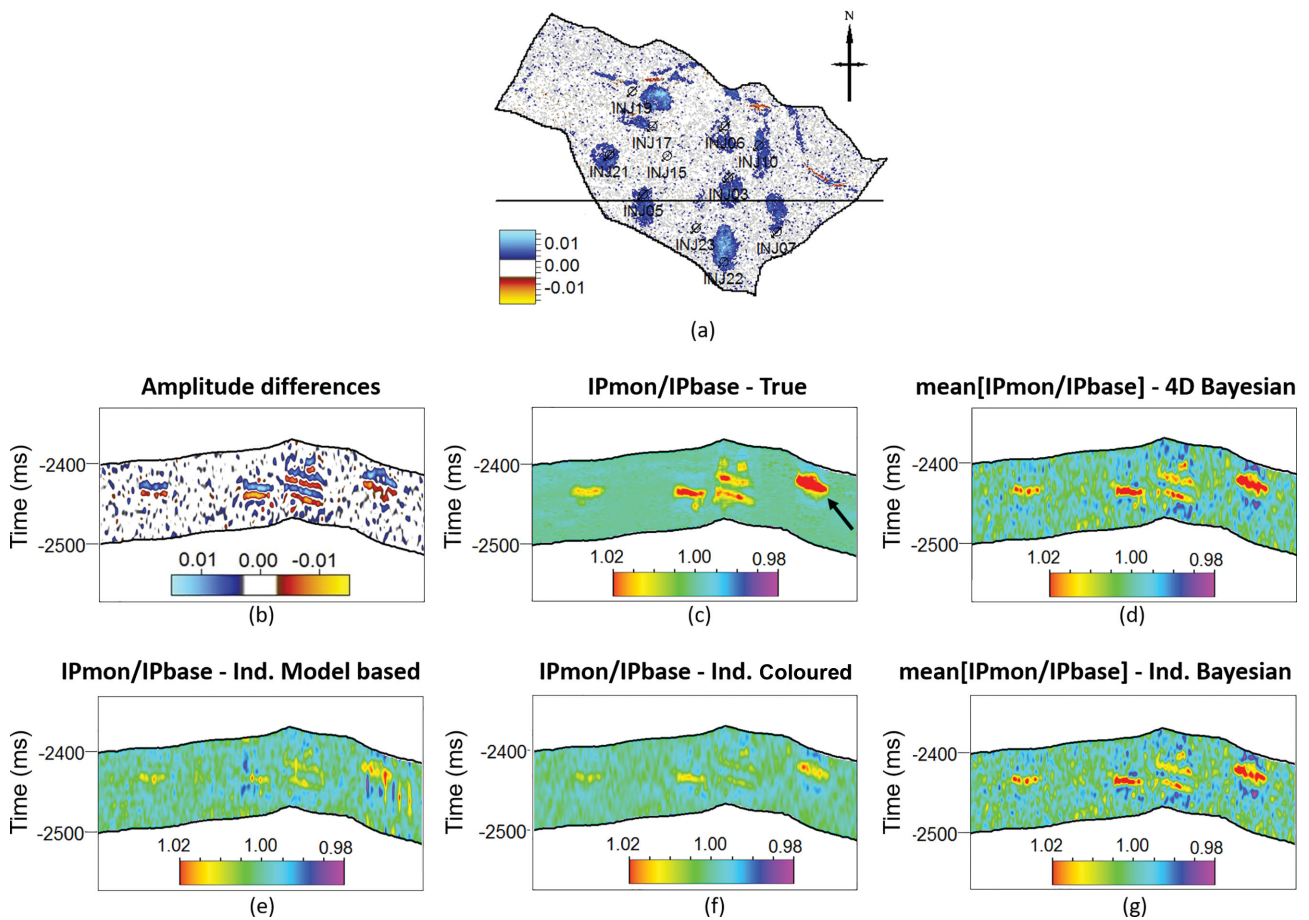


Figure 3. Data visualisation with maps and vertical sections of: (a) impedance ratio and (b) difference in seismic amplitudes. The solid black lines indicate the top and base of the reservoir and the dashed lines indicate the window of RMS maps extraction. The red anomalies in the upper left image represent increased acoustic impedance values caused by water injection from the wells. This increase is seen as blue amplitude anomalies on the lower left image.

pressure, as well as to displace the oil to producing wells due to the pressure gradient. The increase in water saturation caused by water replacing oil results in an increase in the acoustic impedance, and this provides strong 4D anomalies in seismic data. The high-resolution reservoir model is

defined on a grid of  $25 \times 25 \times 1$  m in size. The model includes 25 wells.

To generate the synthetic seismic data from the high-resolution reservoir model, the first step is to generate elastic properties by applying a petro-elastic model to the



**Figure 4.** (a) The dRMS map of the difference in seismic amplitudes with indicated inline for vertical sections; (b) Seismic amplitude differences. The other plots show the ratio  $IP_{\text{monitor}}/IP_{\text{base}}$  of: (c) the true solution; (d) Bayesian 4D joint inversion (median values); (e) model-based inversion; (f) coloured inversion and (g) Bayesian sequential independent 3D inversion (median values). The black lines indicate the top and base of the reservoir. Inline 151. The black arrow in true data shows the anomaly that is analysed in the inversion methods, and the interval of RMS map extraction is defined between two horizons that pass above and below this anomaly. The Bayesian 4D joint approach shows a better lateral continuity of the red anomaly.

petrophysical and dynamic properties of the reservoir model, thus obtaining the elastic attributes ( $V_p$ ,  $V_s$  and  $\rho$ ). The petro-elastic relation that correlates elastic properties with variable fluid saturation and pressure in the reservoir, can be modelled through different methods (Mavko *et al.* 2009). In this case, Gassmann’s equation (Gassmann 1951) and Batzle & Wang (1992) are used to describe saturation changes, whereas the Hertz–Mindlin model describes pressure sensitivity (Avseth *et al.* 2011). The model is then converted from depth to time and resampled from a corner point grid into a regular seismic volume. The elastic attributes can be used to calculate the reflection coefficients using the Aki–Richards approximation and the seismic amplitudes used a convolutional model (Souza *et al.* 2018). Gaussian noise is added to the amplitudes assuming a signal-to-noise ratio of three. This method was used to generate the base (before starting production,  $T = 0$  days) and the monitor survey (after approximately seven years of production,  $T = 2618$  days).

The 4D seismic data difference is the result of the difference between the monitor survey minus the base survey, after time-shift correction.

The wavelet considered is an Ormsby wavelet, and has a trapezoidal shape in the frequency spectrum, defined by the following frequencies: 0, 20, 60 and 80 Hz (figure 2), simulating a broadband seismic acquisition technology (Souza *et al.* 2018). We used it in the forward modelling to generate the synthetic data and in seismic inversion problem.

The difference in seismic amplitudes and the impedance ratio are shown in figure 3 in maps and vertical seismic sections. The seismic amplitudes represent the observed data to be inverted and the impedance ratio is the true solution that the inversion algorithm aims to predict. Figure 3 also shows the spatial pattern of water diffusion. The root-mean-square (RMS) maps are calculated separately for baseline and repeated surveys. Then the dRMS (difference of the RMS:

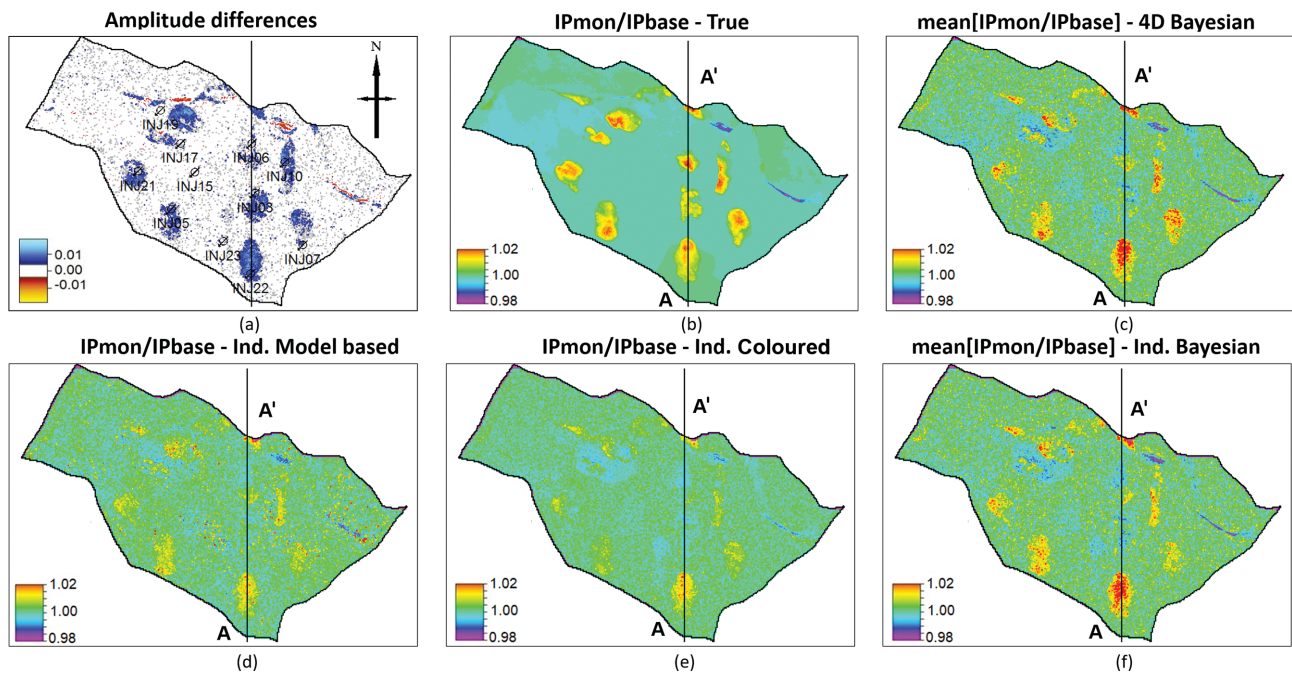


**Figure 5.** (a) The dRMS maps of difference in seismic amplitudes. The other plots show the RMS map of the ratio  $IP_{\text{monitor}}/IP_{\text{base}}$  for: (b) the true solution; (c) Bayesian 4D joint inversion (median values); (d) model-based inversion; (e) coloured inversion and (f) Bayesian sequential independent 3D inversion (median values). The segment A–A’ (vertical black line) indicates the direction of vertical seismic section displayed in Figure 6. The blue anomalies indicate areas around injector wells where water replaced oil, and represent an increase in acoustic impedance ratios (red anomalies). The Bayesian 4D joint approach matches the data solution better than the other methods.

dRMS =  $RMS_{\text{mon}} - RMS_{\text{bs}}$ ) map is obtained, as recommended in Stammeijer & Hatchell (2014). The dRMS maps are shown in figures 4 and 5. For the acoustic impedance cubes, the RMS maps are calculated in the ratio between values of repeated survey and baseline.

The inputs for all the inversions are 3D volumes of monitor and base surveys, the wavelet and horizons of the top and base of the reservoir. For the model-based method, we used sonic and density logs (extracted from the reference model), and interpolated the values across the horizons to build the initial low-frequency model. We also used this prior model for the Bayesian sequential 3D independent inversion. In both methods, the same prior model is considered to invert the monitor and baseline data. Similarly, in the Bayesian 4D joint inversion, the initial model is constant and equal to 0, meaning no 4D changes are previously assumed.

The true solution is known and used for validation in a design of experiments approach. We compare the results using 2D sections, RMS and dRMS maps and crossplots of inversion results against the expected solution.

**5. Results and discussions**

Figure 4 compares the inversion results along a vertical seismic section corresponding to a seismic inline shown on the

map (black horizontal line). Due to the narrowed resolution of seismic data, the inverted results are expected to have a lower resolution when compared to the true data. From a qualitative point of view, the Bayesian inversion methods (figure 4d and g) produced results that are closer to the true data (figure 4c). The time-lapse (figure 4d) and combination of independent 3D (figure 4g) settings of Bayesian inversion presented similar results, but the first showed a better lateral continuity of the highlighted anomaly (black arrow in true data, figure 4c). In all methods, it is possible to see some remaining effects of the wavelet side lobes (from the amplitude data) around the stronger (with higher values) and vertically thicker anomalies. These effects appear above and below the main signals, with opposite values, and their magnitudes depend on the magnitude of the anomaly, i.e., the higher the value of the anomaly, the higher the value of the opposite signal around it.

Figure 5 compares the dRMS map, extracted from the difference of seismic amplitudes, and RMS maps of the ratio  $IP_{\text{monitor}}/IP_{\text{base}}$  for different inversion results, computed in a 10-ms time window. The positive anomalies (blue in figure 5a) in the seismic difference map are correlated to the water injection in the reservoir, whose increase causes positive changes of acoustic impedance in the true data (figure 5b in warm colours). Figure 6 shows a seismic crossline mainly

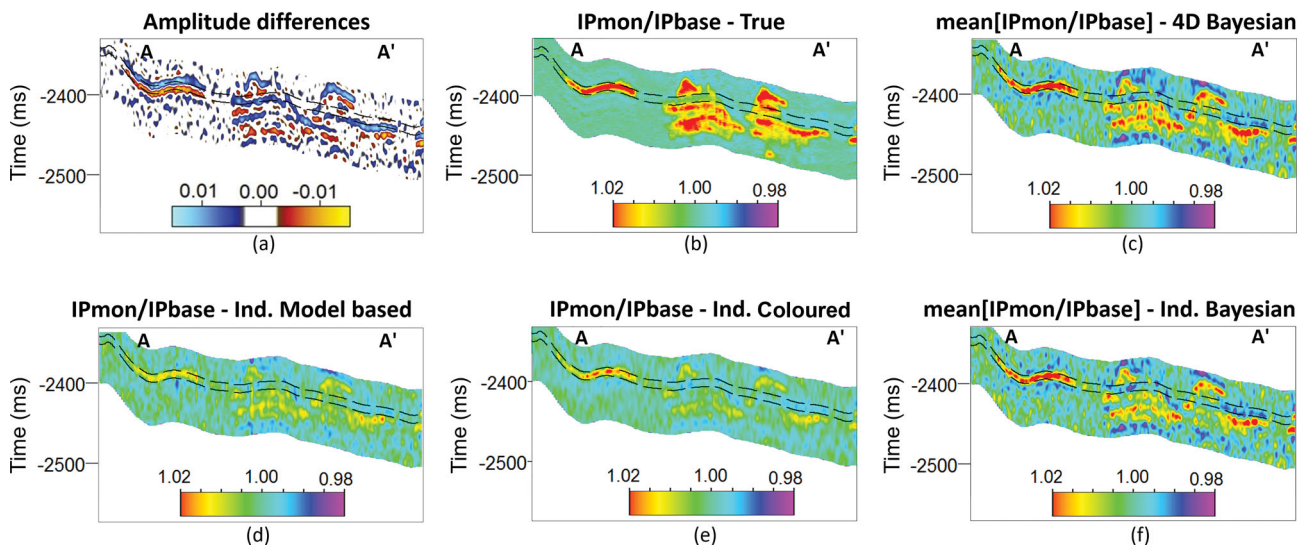


**Figure 6.** (a) Seismic amplitude differences. The other plots show the ratio  $IP_{\text{monitor}}/IP_{\text{base}}$  of: (b) the true solution; (c) Bayesian 4D joint inversion (median values); (d) model-based inversion; (e) coloured inversion and (f) Bayesian independent 3D inversion (median values). The black dashed lines indicate the window of extraction of RMS maps, and the direction of the window is represented by the A–A’ segment. Crossline 191. The shape, value and continuity of red anomalies are evaluated in inverted methods, and checked against true data. The Bayesian 4D joint approach estimates anomalies more accurately. The remaining effects of side lobes are present around the thicker anomalies in all methods, but they are stronger in the Bayesian inversions because of the higher magnitude of their anomalies.

**Table 1.** L2 norm of each inversion method against the true solution.

Inversion technique	L2 norm
4D Bayesian	10.49
Ind. Bayesian	10.82
Ind. coloured	20.19
Ind. model-based	27.71

**Table 2.** MSE values of each inversion method against true solution.

Inversion technique	MSE values
True, 4D Bayesian	0.27373
True, Ind. Bayesian	0.33524
True, Ind. coloured	0.37139
True, Ind. model-based	0.37442

through three anomalies (A–A’ segment in figure 5). Not all anomalies observed in the true data (figure 5b) are recovered by the inversion methods (figure 5c–f). The Bayesian 4D joint approach (figure 5c) retrieves most 4D signals.

The dashed lines in figure 6 represent the window in which the signal was extracted to generate the maps of figure 5. The convolution operation filters the reflection coefficients, causing a loss of resolution in data that cannot be fully recovered by the inversion methods (Russell 1988), and this explains the difficulty in recovering the two anomalies in the centre. Once again, the Bayesian 4D joint inversion provides the best results, whereas the deterministic inversion methods fail to estimate the main anomalies in the true data.

To quantitatively assess the quality of the results, we cross-plot the result of each inversion method against the true data (figure 7), and calculate the L2 norm, whose results are shown in Table 1. Bayesian inversions provide the best correlation between predictions and true data, whereas coloured inversion underestimates the true changes in impedances and model-based inversion exhibits many outliers. The outliers of model-based inversion are related to vertical stripes observed

in seismic vertical sections, which are artefacts caused by the inversion.

The RMS maps used for the similarity calculation between inversions and true data are shown in figure 5 (before standardisation). Figure 8 shows the maps after MSE normalisation (Rollmann et al. 2020), and the corresponding error values are found in Table 2 in ascending order.

The MSE indicator measures the similarity between maps, the lower the error, the closer the method is to the reference. In agreement with previous analyses, the Bayesian 4D joint inversion achieved the best result, but all methods were able to reproduce reliable anomalies (in terms of shape and sign), specially the coloured inversion. We speculate that the more accurate results are due to the vertical correlation model imposed in the Bayesian joint 4D inversion that can be controlled (as an input parameter) to enhance the vertical resolution of the data, allowing it to be closer to the solution (the impedance ratio calculated in the reference simulation model scale with high vertical resolution).

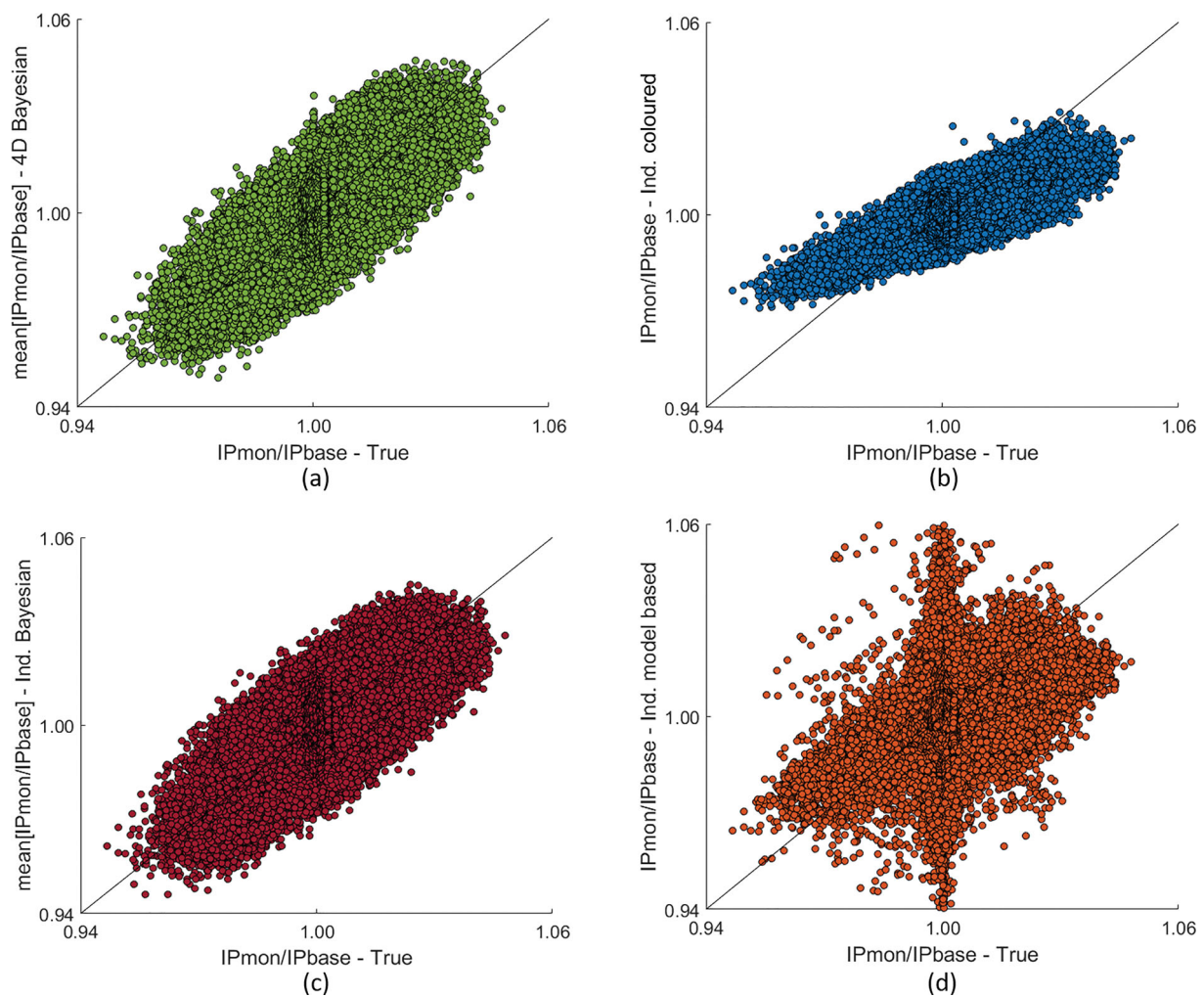


**Figure 7.** Crossplots between the ratio  $IP_{\text{monitor}}/IP_{\text{base}}$  of true data versus: (a) Bayesian 4D joint inversion (median values); (b) coloured inversion; (c) Bayesian independent 3D inversion (median values) and (d) model-based inversion. The identity line is displayed in black for each plot.

## 6. Conclusions

This work shows the comparison of different seismic inversion methods to estimate 4D impedance changes, applied to a benchmark dataset case mimicking waterflooding during production. We compared four methods: Bayesian 4D joint inversion, Bayesian sequential independent 3D inversion, deterministic sequential independent 3D model-based inversion and deterministic sequential independent 3D coloured inversion. All the methods under investigation produce a reliable estimation of the impedance changes that cause the seismic anomalies in the repeated seismic survey. A quantitative analysis shows that the Bayesian 4D joint method is the most accurate in terms of the misfit estimators chosen for the evaluation of algorithm performances. The higher accuracy of the Bayesian 4D joint inversion is desirable, especially in reservoirs with small 4D anomalies where the pre-

cision in the prediction of impedance changes is critical for the decision-making process associated with reservoir production and management.

## Acknowledgements

This work was carried out in association with the ongoing Project (grant no. 20372–9 ANP) ‘Development of integration between reservoir simulation and seismic 4D - Phase 2’ (University of Campinas/Shell Brazil/ANP) funded by Shell Oil Brazil Ltd under the R&D ANP levy as the ‘Investment Commitment to Research and Development’. The authors are also grateful for the support of the Center of Petroleum Studies (CEPETRO-UNICAMP/Brazil), the Department of Energy (DE-FEM-UNICAMP/Brazil), the Research Group in Reservoir Simulation and Management (UNISIM-UNICAMP/Brazil) and Energi Simulation. In addition, special thanks to Bruno Albiero Pazetti, Guilherme Avansi and Klaus Rollmann for their support

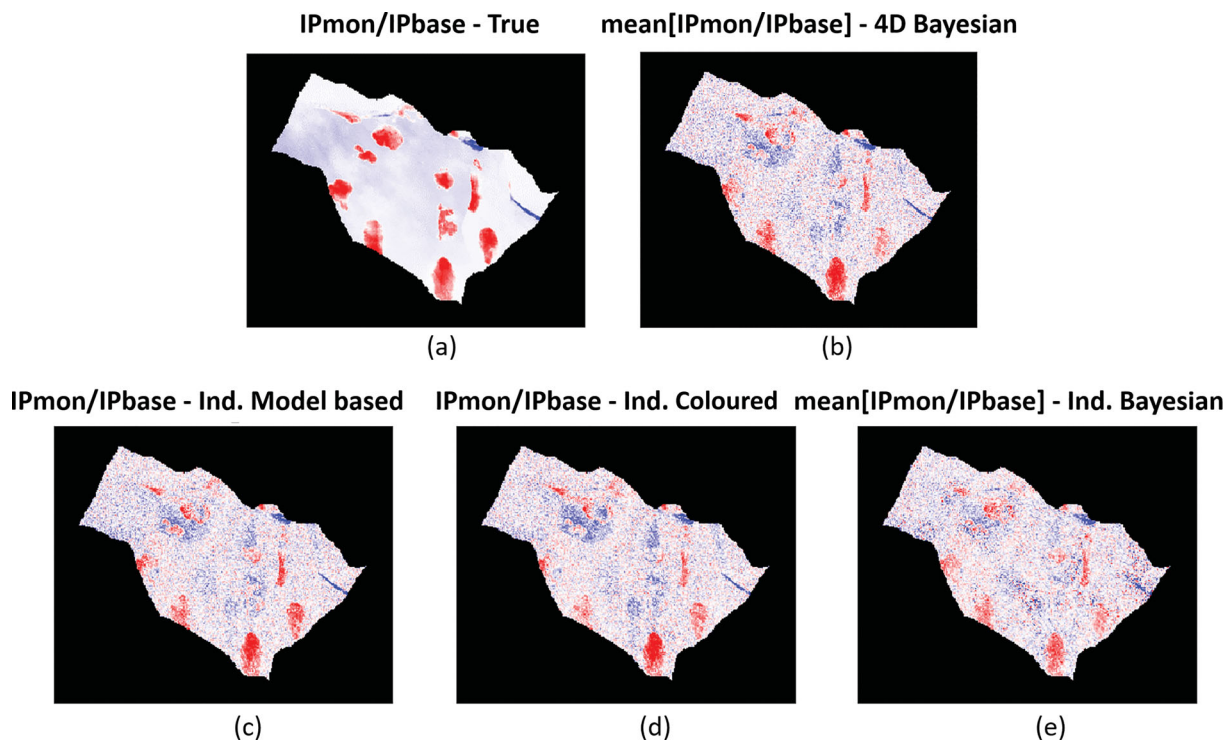


**Figure 8.** Normalised RMS maps of the ratio  $IP_{\text{monitor}}/IP_{\text{base}}$  for: (a) the true solution; (b) Bayesian 4D joint inversion (median values); (c) model-based inversion; (d) coloured inversion and (e) Bayesian sequential independent 3D inversion (median values).

and suggestions, and to Schlumberger, CGG and CMG for software licences.

**Conflict of interest statement:** None declared.

## References

- Aki, K. & Richards, P.G., 1980. *Quantitative Seismology*, W.H. Freeman & Co.
- Avansi, G.D. & Schiozer, D.J., 2015. UNISIM-I: synthetic model for reservoir development and management applications, *International Journal of Modeling and Simulation for the Petroleum Industry*, **9**, 21–30.
- Avseth, P., Mukerji, T. & Mavko, G., 2011. *Quantitative Seismic Interpretation*, Cambridge University Press.
- Bacon, M., Simm, R. & Redshaw, T., 2007. *3-D Seismic Interpretation*, Cambridge University Press.
- Batzle, M. & Wang, Z., 1992. Seismic properties of pore fluids, *Geophysics*, **57**, 1396–1408.
- Buland, A. & El Ouair, Y., 2006. Bayesian 4D joint inversion, *Geophysics*, **71**, R43–R48.
- Buland, A. & Omre, H., 2003. Bayesian linearized AVO inversion, *Geophysics*, **68**, 185–198.
- CGG, 2016. *Post-Stack Inversion Guide*. Software documentation.
- Davolio, A., Maschio, C. & José Schiozer, D., 2014. A methodology to calibrate water saturation estimated from 4D seismic data, *Journal of Geophysics and Engineering*, **11**, 1–16.
- Francis, A., 2005. Limitations of deterministic and advantages of stochastic seismic inversion, *CSEG Recorder*, **30**, 5–11.
- Gassmann, F., 1951. Elastic waves through a packing of spheres, *Geophysics*, **16**, 673–685.
- Grana, D. & Mukerji, T., 2015. Bayesian inversion of time-lapse seismic data for the estimation of static reservoir properties and dynamic property changes, *Geophysical Prospecting*, **63**, 637–655.
- Johnston, D.H., 2013. *Practical Applications of Time-Lapse Seismic Data*, Distinguished Instructor Short Course, Society of Exploration Geophysicists.
- Kazemi, A., Stephen, K.D. & Shams, A., 2011. Seismic history matching of Nelson: an investigation of 4D signature calibration, *SPE Reservoir Evaluation and Engineering*, **14**, 621–633.
- Lafet, Y., Roure, B., Doyen, P.M., Bornard, R., Buran, H. & Smith, A., 2008. Global 4-D seismic inversion and fluid prediction, *70th EAGE Conference Expanded Abstracts*, pp. 5.
- Lancaster, S. & Whitcombe, D., 2000. Fast-track ‘coloured’ inversion, *SEG Technical Program Expanded Abstracts*, pp. 3–6.
- Maurya, S.P. & Sarkar, P., 2016. Comparison of post stack seismic inversion methods: a case study from Blackfoot Field, Canada, *International Journal of Scientific and Engineering Research*, **7**, 1091–1101.
- Maleki, M., Davolio, A. & Schiozer, D.J., 2018. Qualitative time-lapse seismic interpretation of Norne Field to assess challenges of 4D seismic attributes, *The Leading Edge*, **37**, 754–762.
- Mavko, G., Mukerji, T. & Dvorkin, J., 2009. *The Rock Physics Handbook: Tools for Seismic Analysis of Porous Media*. Cambridge University Press.
- Najjar, N.F., Stronen, L.K. & Alsos, T., 2003. Time-lapse seismic programme at Gullfaks: value and the road ahead, *Petroleum Geoscience*, **9**, 35–41.
- Oliver, D.S. & Chen, Y., 2010. Recent progress on reservoir history matching: a review, *Computational Geosciences*, **15**, 185–221.
- Rollmann, K., Vargas, A.S., Almeida, F., Davolio, A., Schiozer, D.J. & Rocha, A., 2020. Convolutional neural network formulation to compare 4D seismic and reservoir simulation models, *IEEE Transactions on Systems, Man and Cybernetics: Systems*, in revision.

- Russell, B. & Hampson, D., 1991. Comparison of post-stack seismic inversion methods, *SEG Technical Program Expanded Abstracts*, 876–878.
- Russell, B.H., 1988. Part 2-the convolutional model, in *Introduction to Seismic Inversion Methods*, Society of Exploration Geophysicists, doi: 10.1190/1.9781560802303.ch2.
- Sarkar, S., Gouveia, W.P. & Johnston, D.H., 2003. On the inversion of time-lapse seismic data, *SEG Technical Program Expanded Abstracts*, 1489–1492.
- Simm, R., Bacon, M. & Bacon, M., 2014. *Seismic Amplitude: An Interpreter's Handbook*, Cambridge University Press.
- Souza, R., Lumley, D., Shragge, J., Davolio, A. & Schiozer, D.J., 2018. Analysis of time-lapse seismic and production data for reservoir model classification and assessment, *Journal of Geophysics and Engineering*, **15**, 1561–1587.
- Stammeijer, J. G. F. & Hatchell, P. J., 2014. Standards in 4D feasibility and interpretation, *The Leading Edge*, **33**(2), 134–140.
- Tarantola, A., 2005. *Inverse Problem Theory and Methods for Model Parameter Estimation*, Society for Industrial and Applied Mathematics.
- Ullmann De Brito, D., Moraes, R. & Emerick, A.A., 2010. The Marlim Field: incorporating time-lapse seismic in the assisted history matching, *SPE Latin American and Caribbean Petroleum Engineering Conference*, doi:10.2118/137763-ms.
- Veeken, P.C.H. & Da Silva, A.M., 2004. Seismic inversion methods and some of their constraints, *First Break*, **22**, 47–70.
- Veire, H.H., Borgos, H.G. & Landrø, M., 2006. Stochastic inversion of pressure and saturation changes from time-lapse AVO data, *Geophysics*, **71**, C81–C92.
- Wang, Y., 1999. Approximations to the Zoeppritz equations and their use in AVO analysis, *Geophysics*, **64**, 1920–1927.
- Wang, Y., 2003. *Seismic Amplitude Inversion in Reflection Tomography*, Pergamon-Elsevier, Oxford.
- Wang, Y., 2016. *Seismic Inversion, Theory and Applications*, Wiley Blackwell, Oxford.